Measurements of Temperature and Enthalpy in NASA Ames 60-MW Arcjet using Atomic Oxygen and Atomic Nitrogen Absorption

Peter M. Finch*, Zev N. Granowitz †, Christopher L. Strand‡, and Ronald K. Hanson§
High Temperature Gasdynamics Laboratory, 452 Escondido Mall, Bldg. 520, Thermosciences Division, Stanford University, CA 94305, USA

Megan E. MacDonald¶
NASA Ames Research Center, Moffett Field, California 94035, USA

We report on measurements of temperature and enthalpy in the 60-MW Interaction Heating Facility (IHF) Arcjet at the NASA Ames Research Center. These quantities were measured at sub-second temporal resolution using tunable diode laser absorption spectroscopy, employing four Distributed Feedback (DFB) lasers to simultaneously probe the arcjet flow. Optical access was achieved through a specially-designed optical disk mounted in series with the modules of the arc heater in the add-air plenum of the column, which is positioned between the downstream electrodes and the nozzle. Gas at this measurement location serves as the reservoir condition for the ensuing supersonic expansion. Conditions in the reservoir are extreme, with temperatures between 5000-8000 K and pressures between 1-9 atm. Absorption from the ^{5}S state of atomic oxygen at 777.2 nm and the ^{4}P state of atomic nitrogen at 868.0 nm, two electronically-excited quantum states, formed the basis of the flow characterization measurements. Fiber-coupled laser light was pitched through the IHF via 1/8" ports in the optical disks, permitting optical access with minimal intrusion to the flow. Data was collected at 3 nominal conditions, a Low condition (1600 A, 2000 V, 0.13 kg/s), a Medium condition (3500 A, 5700 V, 0.61 kg/s), and a High condition (5900 A, 6800 V, 0.84 kg/s). Measurements suggest agreement within 1-2% between excited oxygen and excited nitrogen thermometry, indicating approximate thermal and chemical equilibration of the arcjet reservoir state, a result in keeping with long-standing assumptions of CFD modelling. Spatial gradients are found in the flow due to enthalpy loss to the facility walls, but the measured spatial non-uniformities are consistent with axi-symmetry. Measurements of specific enthalpy in the reservoir are also made utilizing excited oxygen and excited nitrogen absorption under the assumption of chemical equilibration.

Keywords: Arcjet, NASA Ames, hypersonic flows, reentry, laser absorption spectroscopy, thermometry, electronic excitation

I. Nomenclature

A	=	integrated absorbance [cm^{-1}]
A_{21}	=	Einstein A [s^{-1}]
c	=	speed of light [cm/s]
E	=	lower-state energy [cm^{-1}]
g	=	degeneracy
k_B	=	Boltzmann constant [J/K]
λ	=	wavelength [cm]

*Graduate Student, Mechanical Engineering, AIAA Member, Corresponding Author, pmf277@stanford.edu
†Graduate Student, Mechanical Engineering
‡Senior Research Engineer, Mechanical Engineering, AIAA Member
§Clarence J. and Patricia R. Woodard Professor of Mechanical Engineering, AIAA Fellow
¶Aerospace Engineer, AIAA Member

L	=	optical path length [cm]
n	=	number density [1/cm^3]
ν	=	frequency [cm^{-1}]
Φ	=	lineshape function [cm]
Q	=	partition function
S	=	linestrength [cm^{-2}/cm^3]
T	=	temperature [K]

II. Introduction

This work is a part of an ongoing collaborative effort between NASA and Stanford University to characterize the 60-MW Interaction Heating Facility (IHF) Arcjet at the Ames Research Center [1, 2]. The IHF facility, and the Ames Arcjet Complex broadly, have served a vital role in the testing and development of thermal protection systems (TPS) for hypersonic, planetary entry, and Earth reentry applications over many decades [3–6]. Spacecraft re-entering Earth's atmosphere, or entering the atmosphere of another planet, may do so at orbital or hyperbolic speeds. At these high Mach numbers, flows impinging on the vehicle develop strong shockwaves with large post-shock temperatures. TPS materials must be robust to withstand these hazardous hypersonic flow environments over the span of many minutes. Given the extremities of convective heating to the vehicle body, many TPSs are over-designed at a weight penalty [7]. Ground testing serves an essential role in vigorously testing TPS materials to ensure they can safely and efficiently withstand the intended entry trajectory[8–10]. Amongst hypersonic ground testing facilities, arcjets have the favorable characteristic that they permit long test times at durations that are often orders of magnitude longer than impulse facilities[11, 12]. This is a particularly advantageous trait when investigating structural heating during reentry.

The IHF is a high-power, large-scale segmented arcjet facility at NASA Ames. The facility consists of two electrode packages, an anode and a cathode, separated by a constrictor tube comprising a series of modules which, in turn, are made up of individual water-cooled copper disks [13, 14]. During the operation of the facility, high voltage imposed across the electrodes induces the breakdown of the test gas in the arc column, permitting the transference of electrical power into the internal energy of the flow. The test gas in the IHF is dehydrated atmospheric air, with an argon buffer to assist in the initiation of the discharge. After the electrode packages, the flow passes by the add-air plenum, whereby room-temperature air is injected into the arc-heated gas in order to provide additional tunability to the tailoring of the flow enthalpy. The intersection of the two gas sources induces turbulent mixing, but this mixing requires sufficient length to homogenize. The length of this mixing volume, and the ensuing loss of flow enthalpy that it precipitates, has been the primary concern of previous work [1, 2]. After the mixing volume, the flow is expanded through a conical nozzle to supersonic velocities into the test chamber. The flow in the mixing section is thus the reservoir condition that sources this ensuing supersonic flow. In the test chamber, TPS test articles are secured on sting arms and inserted into the jet, thereby simulating the entry or reentry environment.

Several gradations of input electrical power are possible, which are manifested in the conditions of the flow in the reservoir and the test chamber. In this paper, we refer to three such conditions, the Low condition, the Medium condition, and the High condition. Such a nomenclature is somewhat simplistic, as the IHF functions at a continuum of possible conditions, and though the runs presented in this work fell into the aforementioned ranges, not all runs do, nor are runs at alike conditions exactly the same (see Figs 5, 6, and 7). This variability is not a deficiency, but rather a biproduct of the IHF operators finely tuning the arc to achieve the conditions required for any given test model.

Over the operational range of the IHF, the arc heater can generate temperatures of 5000-8000 K and pressures of 1-9 atm in the reservoir. It is in this region of the flow that optical measurements were taken. Optical access through the column was achieved through specially designed disks just downstream of the add-air ports. Given the elevated temperatures in the reservoir, the flow is significantly dissociated. The primary target species for measurement were thus atomic oxygen and atomic nitrogen, the latter being a new inclusion in this work. As in the previous studies, laser absorption spectroscopy was utilized to characterize the temperature, composition, and enthalpy of the IHF flows. The laser system employed was significantly improved, however, providing higher signal to noise, enhanced temporal resolution, and an expanded spatial range of measurements. These improvements, along with the measurement of a new species (N*), allow for greater confidence in the reservoir condition and its spatial/chemical uniformity. This was a primary goal of this research, mindful of the immense importance of known reservoir conditions in order to understand the characteristics of the resulting freestream flow that impinges on the test article [15–17].

III. Spectroscopic Theory

In this work, Scanned Direct Absorption (Scanned DA) is used to infer the temperature and composition of the reservoir gas. In Scanned DA, monochromatic laser light is pitched across an absorbing gas medium. By modulating the injection current of the laser in a periodic fashion, the resulting wavelength of this monochromatic light changes periodically as well. When the wavelength is resonant with certain quantum mechanical state transitions between internal energy levels of the absorbing gas, the light is partially absorbed. This absorption is noted by a dip in transmitted intensity on a receiving photodetector. Via the Beer-Lambert relation [18], the negative natural log of the ratio of the transmitted light intensity versus the input light intensity is defined as the absorbance. Due to quantum mechanical effects and the thermal motion of gases, the absorbance of a transition is dispersed over a range of wavelengths, an effect known as broadening. By spectrally integrating the absorbance, the absorbance loses its dependence on lineshape, Φ, and can be calculated in Eq 1. For a transition, i, of absorbing species, j, the integrated absorbance is a function of the temperature dependent linestrength, S_i, the number density of the species, n_j, and the pathlength, L. If the absorbing medium is spatially varying across the pathlength, Eq 1 can be discretized along the pathlength, or the absorbance can be treated using path-averaged quantities.

$$A_i = \int_{-\infty}^{\infty} n_j L S_i(T)\Phi_i(T,P,\nu)d\nu = n_j L S_i(T) \tag{1}$$

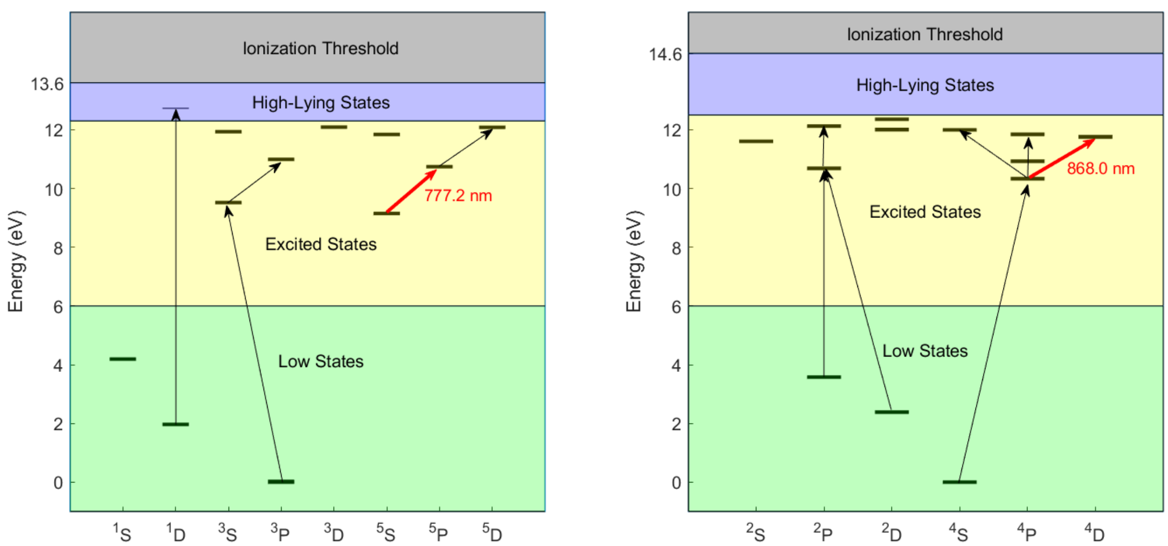

(a) Energy states of O

(b) Energy states of N

Fig. 1 Simplified energy level for atomic oxygen (left) and atomic nitrogen (right). States are denoted by their term symbol and energy above ground. Arrows denote common transitions between energy levels (by no means comprehensively). The two transitions used in this work at 777.2 nm and 868.0 nm are highlighted in red. For both O and N, the ground state is accompanied by two nearby metastable states that are spin-forbidden to the ground. After a gap in energy of about 5-6 eV, a large collection of excited states reside in the region 9-12 eV above ground. It is here that the ^{5}S and ^{4}P states are found. Above this region is a near-continuum of many energy states (which are not individually denoted) up to the ionization limit.

Linestrength is a function of several spectroscopic variables: the Einstein A parameter, $A_{21,i}$, the upper and lower state degeneracies, $g_{2,i}$ and $g_{1,i}$ respectively, and the transition wavelength, λ_i. These parameters determine the intrinsic strength of a given transition. The dependence on temperature is captured in the Boltzmann fraction, whereby population in a state with internal energy E_i'' is weighted against all other possible states through the partition function Q_j. The values for the above variables are sourced from extensive tabulation by NIST [19], and the partition function is calculated from Irwin [20].

$$S_i = \frac{\lambda_i^2}{8\pi c} \cdot \frac{g_{2,i}}{g_{1,i}} \cdot A_{21,i} \cdot \frac{\exp\left(-E_i''/(k_B T)\right)}{Q_j} \cdot (1 - \exp\left(-\Delta E_i/(k_B T)\right)) \tag{2}$$

The primary spectroscopic targets in this work are atomic oxygen (O) and atomic nitrogen (N), two species that are abundant in the arcjet reservoir. Absorption by atomic species almost always takes the form of electronic transitions from one quantum mechanically permissible electronic configuration to another. However, the ground electronic states of these two species are challenging to monitor spectroscopically, as transitions that emanate from them are either spin forbidden or deep in the ultraviolet range. In this work, we therefore monitor two electronically excited states of O and N. For O, the state $^5S^*_2$ 9.1 eV above ground (henceforth referred to as O*) is probed via its transition at 777.2 nm to the upper state $^5P_3$. Similarly for N, the state $^4P_{5/2}$ 10.3 eV above ground (N*) is probed via its transition at 868.0 nm to the upper state $^4D^*_{7/2}$. The energy level diagrams for O and N are depicted in Fig 1.

The excitation of electronic states is an active research area and comprises several uncertain processes [21, 22]. Reliance on measurements of electronically excited states as a marker of the abundance of a species is thus a dubious undertaking in many circumstances. In the context of arcjet flows, however, this assumption may not be so ambitious. Given the high temperatures, high pressures, and sustained conditions over the span of minutes, the flow should achieve thermal equilibrium with its electronic states, particularly those safely below the Rydberg states. Additionally, the equilibrium assumption should be applicable to chemical composition as well. These two assumptions permit the notion of "single-line thermometry", whereby the two unknowns, S_i and n_j, in Eq 1, can be determined from a single measurement under the constraint of thermal and chemical equilibrium. A single temperature specifies both the chemical composition of the gas (n_j) given initial conditions, as well as the Boltzmann fraction of internal energy states within a given species, thus dictating S_i. It is still necessary to know the total number density of the gas in order to distinguish higher absorbance due to stronger linestrength versus that from larger overall bulk density. This additional measurement is provided by the IHF instrumentation, which records both pressure and mass flow rate. Also implicit in this type of thermometry is the uniqueness of any given combination of S_i and n_j. While absorption will always rise if the number density increases, the linestrength is in general a non-trivial function of temperature. However, over the applicable temperature and pressure range of arcjet conditions, the linestrength of both the O* and N* transitions are monotonic, as shown in Fig 2.

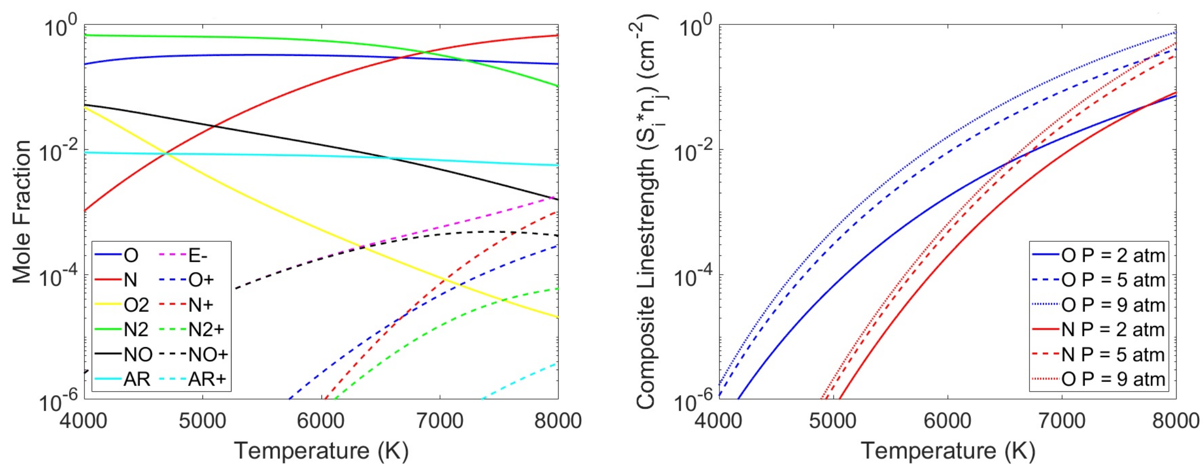

(a) Equilibrium air at 2 atm

(b) Linestrength of O* and N* transitions

Fig. 2 Left: Equilibrium mole fraction calculations of air at 2 atm across the temperature spectrum of the IHF facility. Equilibrium calculations are made according to the NASA-9 polynomials [23]. Right: The linestrengths of the O* 777.2 nm line and N* 868.0 nm line. These calculations are made given the equilibrium composition of the gas, the Boltzmann fractions of the particular lower states, and the spectroscopic constants from [19]. The linestrengths as plotted are 'composite', in the sense that they are population dependent (i.e. $S_i * n_j$). Both transitions exhibit monotonic behavior in this temperature and pressure regime, indicating that any observed absorbance over a known pathlength and static pressure maps uniquely to a single temperature condition.

IV. Experimental Methods

Absorption measurements in this study were obtained by aligning laser light through the IHF. This was accomplished through the use of optical probes which attached to the arc column in the IHF add-air plenum. The facility accommodated these probes with specifically-designed optical disks that were deployed in series with the standard add-air disks, as shown in Figure 3. There were four such optical disks, labelled 1-4, and each had four lines of sight (LOS), labelled A-D. In this nomenclature, B is the centerline position, A and C are 1" above and below centerline respectively (sometimes referred to as intermediate), and D is 2" below centerline and closest to the wall. In this study, the four lines of sight on Disk 4 specifically were monitored, enabling simultaneous scanned DA measurements across the diameter of the arcjet. Additional measurements on lines of sight dispersed across other disks will be discussed in a future manuscript.

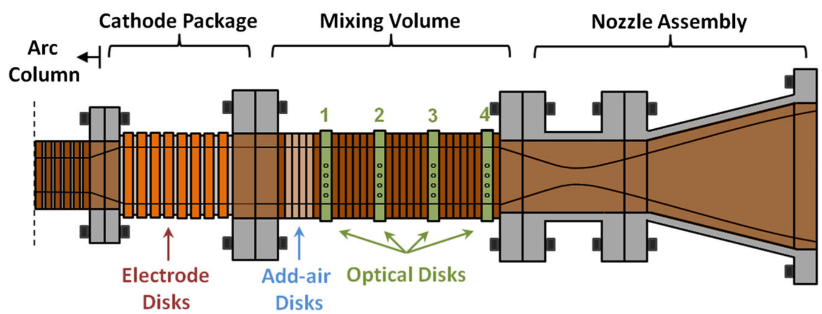

(a)

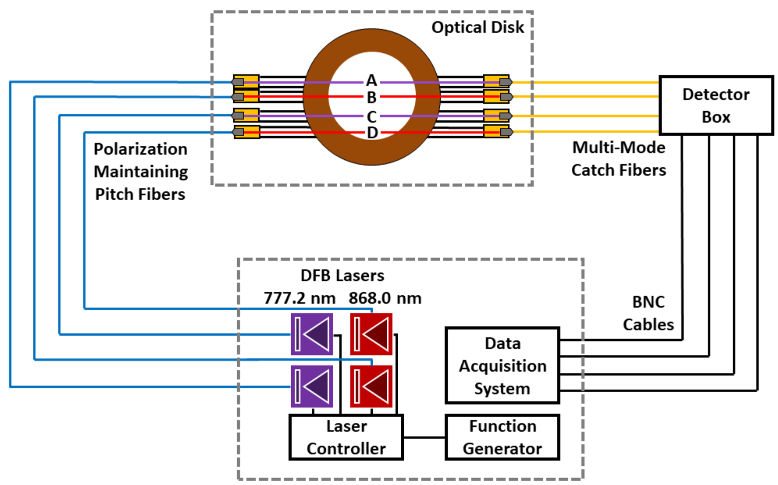

(b)

Fig. 3 Top: Image taken from [2], depicting the add-air section of the IHF. Four disks, numbered 1-4 from upstream to downstream, each have four optical ports, labelled A-D from top to bottom. The optical disks are downstream of the add-air disks and upstream of the nozzle. Disk 4 is thus the final measurement location of the IHF reservoir prior to supersonic expansion into the test chamber. Bottom: A schematic of the optical setup. Four DFB lasers, two at 777.2 nm and two at 868.0 nm, are fiber-coupled into polarization maintaining fibers, which are pitched across the column from the optical ports. Light is collected on multi-mode fibers and fed into photodetectors. These signals are recorded on the data acquisition system in real time during the run.

In the previous works [1, 2], a 50 mW New Focus^{TM} External Cavity Diode Laser (ECDL) was the primary light source. Targeting O* at 777.2 nm, this laser was coupled through a fiber-splitter and split onto the four A-D paths. In this work, four new 20 mW Distributed Feedback (DFB) lasers from Nanoplus^{TM} were employed. Two of the DFB lasers were centered at 777.2 nm to measure O*, while the other two were centered at 868.0 nm to measure N*, the latter being a new target in this work. The most common configuration of the laser system was to align the two O* lasers on two of the lines of sight and to have the N* lasers occupy the other two. If the duration of the run was sufficiently long, the configuration was 'swapped' mid-run, whereby the O* and N* lasers would interchange their respective lines of sight. This swapping was conducted when the facility had already achieved its condition and was nominally steady, permitting the comparison of measurements on either end of the swap. In other cases, if the run duration was not long enough, the lines of sight were swapped in between runs of the same nominal condition. The results in this manuscript employ the latter swapping method.

All four lasers were scanned at rate of 1 kHz and fiber-coupled into polarization-maintaining, single-mode optical fibers (PM780-HP, 5 μm core diameter, 0.13 numerical aperture (NA)) from Thorlabs$^{\text{TM}}$. Fiber delivery of light into the IHF permitted laser light to be fully enclosed and supporting electronics to be kept at a safe distance from the extreme electrical power of the arc heater. The fibers coupled to the DFB lasers terminated at the aforementioned optical probes inserted into the arcjet's optical disk. The probes allowed for adjustment of beam alignment and recollimated the beam using fiber-coupled achromatic lens collimators with a 0.50 NA and 8.00 mm focal length, resulting in an approximate output beam diameter through the column of 1.5 mm. After passing through the flow, the beams were caught on a reciprocal set of four probes, which refocused the beams into multi-mode fibers (400μm core diameter, 0.48 NA). Thorlabs$^{\text{TM}}$ PDA-36A switchable gain silicon detectors were placed at the other end of the multi-mode fibers, intervened by narrow band-pass filters (center frequency: 780 nm, FWHM: 10 nm, and center frequency: 870 nm, FWHM: 10 nm) to reduce emission noise. Voltage output from the detectors was recorded at a sampling rate of 5 MHz with a National Instruments$^{\text{TM}}$ PCI 6110 DAQ. Absorption measurements were recorded in 15, 30, or 60 second increments during the ramp-up of the arcjet and at multiple points throughout the test time.

V. Results

A. Raw Data

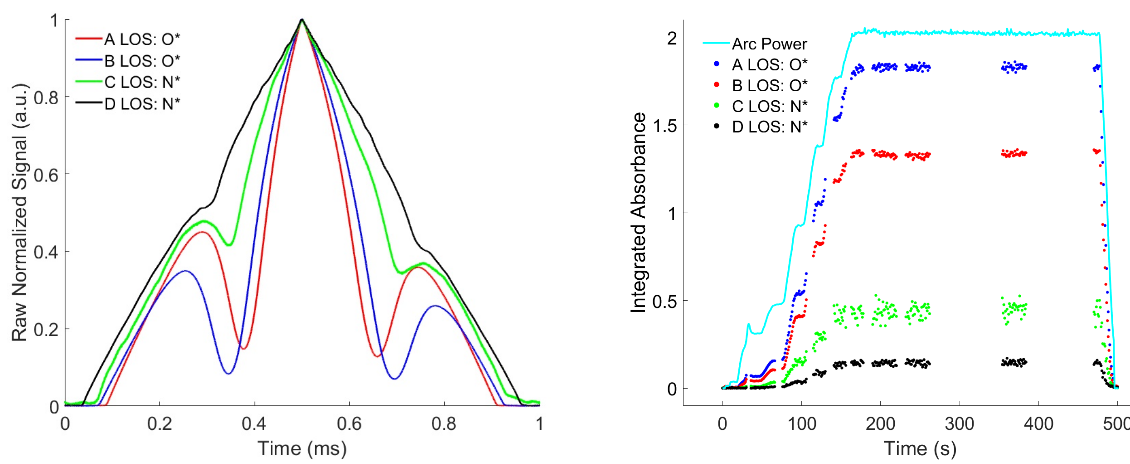

(a) Scan average at High condition

(b) Absorbance time histories at High condition

Fig. 4 Left: Raw data collected from the High condition, with O* beams on the A and B lines of sight and N* beams on the C and D lines of sight. Each laser is scanned with a 1kHz triangular waveform, corresponding to changes in both laser power and wavelength. Dips in the waveform correspond to absorption by O* or N*. At the conditions of the IHF, N* absorbance is almost universally weaker than O* due to spectroscopic effects. In addition, absorption should decrease closest to the relatively cold wall, such that LOS D should be the weakest, all else equal. The data is plotted over the 1 ms time corresponding to a single scan, but is a 100 scan average (representing a temporal range of 100 ms). The raw signal has also been normalized. Right: Integrated absorbance time histories for the same run as on left. Each transition is fit with a Voigt lineshape model, and its integrated absorbance is extracted. Considerable transience in absorbance is evident during ramp-up and ramp-down of the arc, but measurements are stable during test time. Super-imposed is the measured IHF voltage scaled to fit on the plot.

Fig 4 provides a sample of raw data taken during a run at the High condition of the IHF. The lasers are modulated at 1 kHz with a triangle injection current, which in turn changes the output power and wavelength periodically and roughly linearly. Increases and decreases in detected power thus correspond to spectral movement of the lasers, and the laser wavelengths can momentarily coincide with the wavelengths of the probed transitions. This can be seen as dips in the detected power on the photodetector due to photons absorbed along the beampath. This absorption is ultimately fit with a lineshape model, in this case a Voigt lineshape, to determine the integrated absorbances in Eq 1. Time histories of the integrated absorbance for a typical run at the High condition are also shown in Fig 4. In this run, all four lasers were arranged on Disk 4 (see Fig 3), the 777.2 nm lasers targeting O* on LOS A and B, and the 868.0 nm lasers targeting N* on LOS C and D. Due to several spectroscopic effects, the O* transition is stronger than the N* line given the same gas conditions, and absorption from lines of sight closest to the centerline (B) is also higher because the flow is hotter. Co-plotted is the Arcjet heater power in arbitrary units. The heater is ramped up incrementally through several intervening conditions before arriving at the desired condition. This ramping is observed in the transience of the absorbance time histories. The absorbance is steady when the arc achieves its condition in the middle of the measurement window. Gaps in the absorbance time histories are sections where data was not collected. At the end of the measurement window as the IHF ramps down, the absorbance declines until the arc is shut off.

For each modulation period, two measurements per beampath are possible, one on the 'up' scan, and one on the 'down,' for a theoretical measurement rate of 2 kHz. Practically, such a high measurement rate is not necessary, particularly when the IHF achieves its condition, because there is minimal drift in the mean properties of the flow. Typically, averages over several scans are performed to improve measurement quality and help improve signal-to-noise ratios. Noise sources in the data come primarily from two sources: facility vibration which disturbs alignment, and fluctuations in the flow itself. This latter effect manifests both in variation of the emission noise profile as well as oscillations in the magnitude of the line of sight absorbance, which will be investigated in a future work. The combined noise from these sources can sometimes be significant, but they typically have steady mean values, permitting their removal via averaging.

Table 1 Arc heater setpoints for three conditions considered in this study, referred to as High, Medium, and Low. The IHF test series and run number are provided. Pressure refers to measurements in the add-air section, the closest station to the laser lines of sight. Flow rates of main air, add air, and argon are also provided. Values given represent average values during test time.

Condition	IHF Test - Runs	Current (A)	Voltage (V)	Pressure (kPa)	Main (g/s)	Add (g/s)	Argon (g/s)
High	999FCO - 093/4	5900	6800	780	740	50	55
Medium	382 - 003/4	3500	5700	520	520	55	40
Low	389 - 002/3	1600	2000	90	70	50	10

B. High Condition

In Fig 5, the measured path-averaged temperatures from O* and N* absorbance from the High condition on Disk 4 are plotted. The IHF High condition test duration is not typically long enough to permit laser swapping while at-condition. The data in Fig 5 is thus an aggregate of two consecutive runs at this condition on the same day, IHF test series 999FCO, runs 093 and 094 (see Table 1). For the first run, the beams were arranged as described in Fig 4; this arrangement was inverted for the subsequent run. At the bottom of Fig 5, facility-provided measurements of arc current, arc voltage, mass flow rates, and pressure are plotted from both of the two runs. Despite different test durations, runs 093 and 094 agree very closely during ramp-up and when at nominal condition, permitting quantitative comparison of the lines of sight between the two runs. While it is possible to infer temperature across the entire measurement window of the IHF runs, temperature is reported in Fig 5 over a smaller range coinciding with test time and ~1 minute beforehand. Measurements are recorded at somewhat different moments of time in the two runs, as can be noted in the different recording times of the data points.

Several observations can be made from the data in Fig 5. The first is that temperature decreases from the centerline to the wall (B to D), a result that matches expectation as well as previous measurements in the prior works [1, 2]. Agreement between LOS A and C is also noteworthy, as these two lines of sight are equidistant from the centerline of the column. This finding suggests spatial uniformity of the flow at Disk 4, indicating the success of the mixing length in homogenizing the reservoir prior to nozzle expansion. The uncertainty in the O* temperature measurements, on the order of 50-100 K, is sufficient to demarcate temperature across the three radial locations beyond uncertainty, which represents an improvement from the prior works. The error bars on the N* temperature measurements are usually larger, owing to the former's weaker linestrength and correspondingly smaller absorbance. Comparing O* and N* measurements, there is significant similarity in the inferred temperature field across the lines of sight. The relative spread between lines of sight are also comparable: there is ∼100 K discrepancy between LOS B and LOS A/C and ∼150 K discrepancy between LOS A/C and LOS D as seen in both species. However, the measurements of N* suggest a flow field that is universally higher by ∼100 K. Given the high temperature and pressure at the measurement location driving the flow to equilibrium, this result is surprising. On the other hand, the discrepancy is relatively small (on the order of 1.5%), and is smaller still when considering the combined uncertainties of the two temperature measurements. Should the N* and O* temperatures differ, this result would not be without precedent. Previous IHF measurements in emission have found that both N* and O* states emit at intensities characteristic of temperatures distinct from CFD prediction, as well as dissimilar from each other [24, 25]. Further experimentation is required to verify if this discrepancy persists across repeated runs.

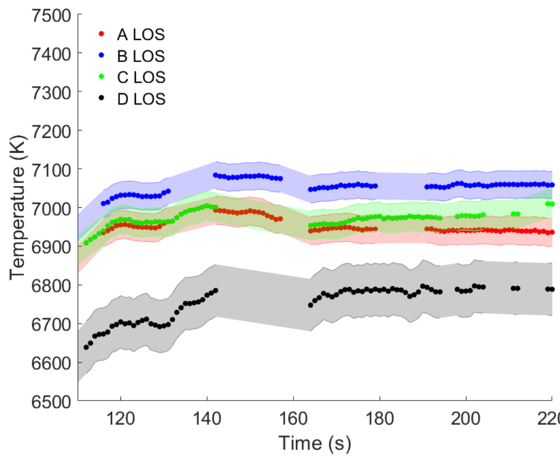

(a) Inferred temperature from O* at High condition

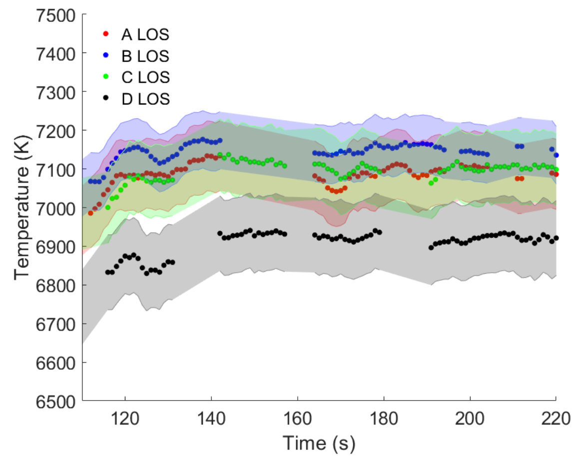

(b) Inferred temperature from N* at High condition

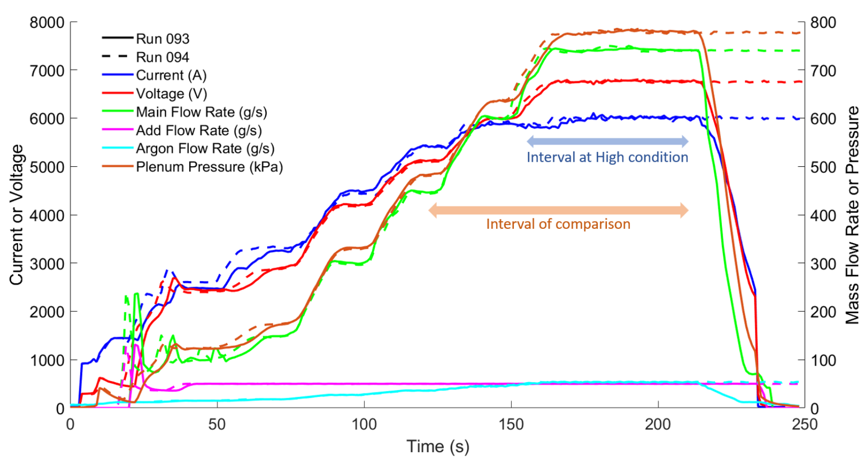

(c)

Fig. 5 Measurements of the temperature at Disk 4 at the High condition (roughly 5900 A, 6800 V, 0.84 kg/s total flow rate) using O* absorption (left) and N* absorption (right). Measurements are combined from two sequential runs of the IHF. In the first run, O* beams occupied LOS A and B and N* beams occupied LOS C and D. Between runs, this arrangement was inverted. Temperature measurements are constrained to around the test times of the respective runs, when the IHF achieved and sustained the High condition. At bottom, facility-recorded traces of current, voltage, pressure, and flow rate based on nominal input values, with time interval at-condition denoted.

C. Medium Condition

In Fig 6, the measured path-averaged temperatures from O* and N* absorbance from the Medium condition on Disk 4 are plotted. Like Fig 5, Fig 6 is an aggregate of two consecutive runs of the Medium condition, IHF test series 382, runs 003 and 004. For the first run, the beams were arranged with N* beams on LOS A and LOS B and O* beams on LOS C and D. This configuration was inverted for the second run. At the bottom of Fig 6, facility-provided measurements are again plotted. The time interval of comparison at condition is longer in Fig 6 relative to Fig 5 owing to the longer test durations typically run at the Medium condition. Results in the Medium condition are ~300-400 K cooler than the High condition. Temperature trends between lines of sight and between O* and N* are otherwise very similar. Measurements again suggest successful homogenization of the reservoir flow, as agreement between the equidistant A and C lines of sight holds within uncertainty across the majority of test time and two different runs. N* inferred temperature is again hotter than the O* temperature, at this condition by ~2%.

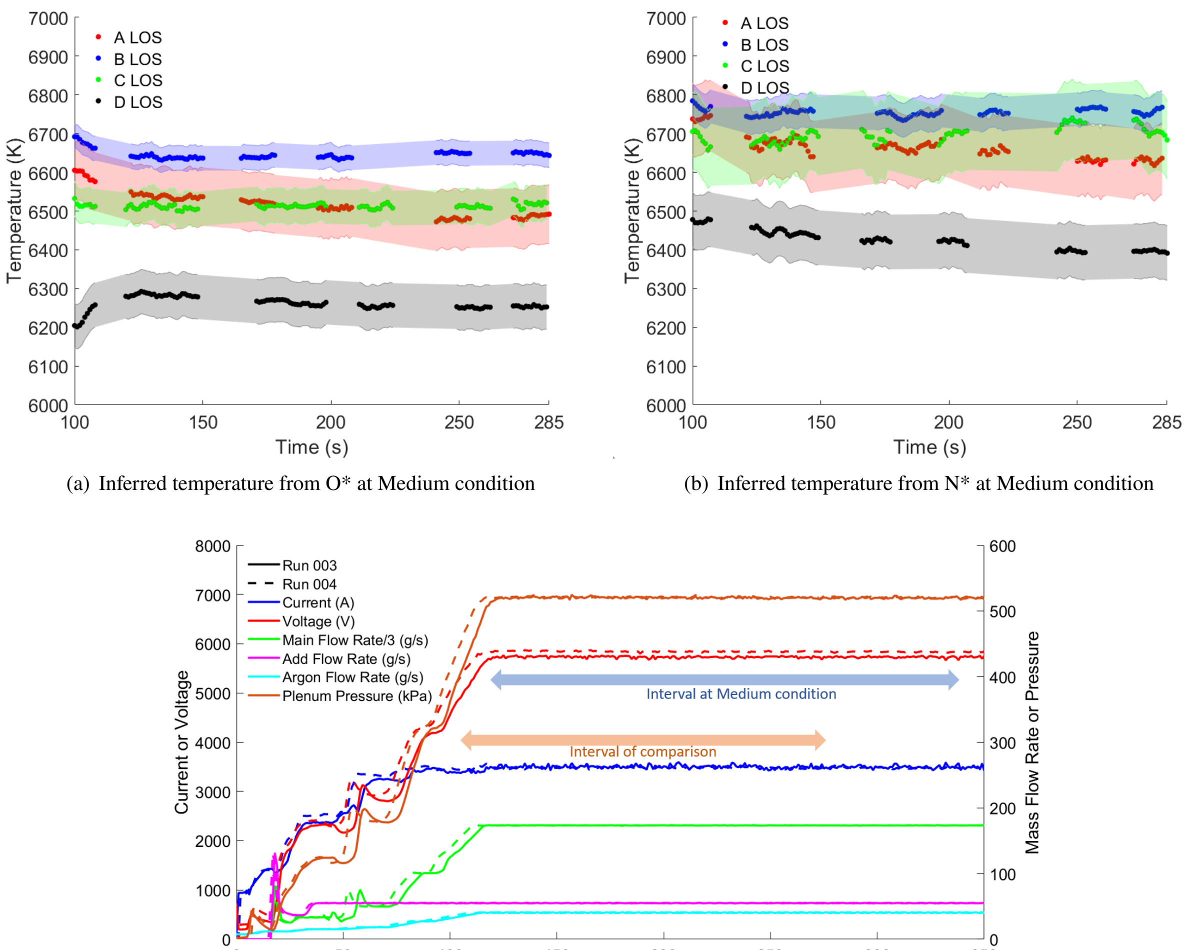

(a) Inferred temperature from O* at Medium condition

(b) Inferred temperature from N* at Medium condition

(c)

Fig. 6 Measurements of the temperature at Disk 4 at the Medium condition (roughly 3500 A, 5700 V, 0.61 kg/s total flow rate) using O* absorption (left) and N* absorption (right). Measurements are combined from two sequential runs of the IHF. In the first run, N* beams occupied LOS A and B and O* beams occupied LOS C and D. Between runs, this arrangement was inverted. Temperature measurements are constrained to around the test times of the respective runs, when the IHF achieved and sustained the Medium condition. At bottom, facility-recorded traces of current, voltage, pressure, and flow rate based on nominal input values, with time interval at-condition denoted.

D. Low Condition

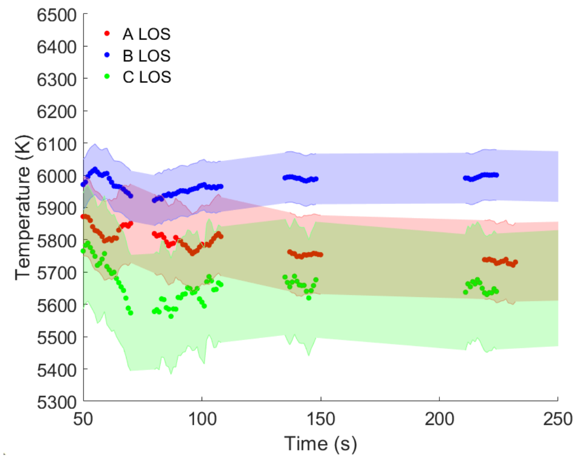

(a) Inferred temperature from O* at Low condition

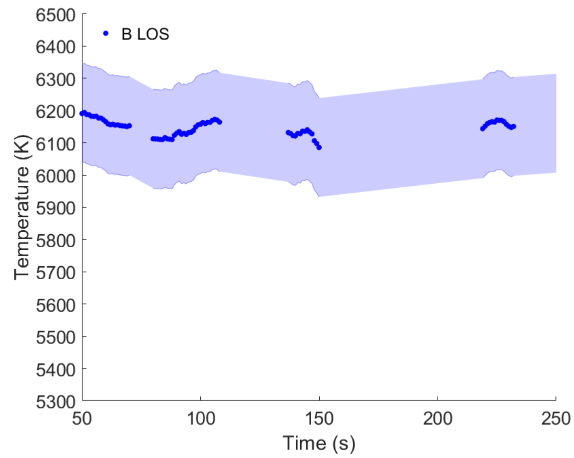

(b) Inferred temperature from N* at Low condition

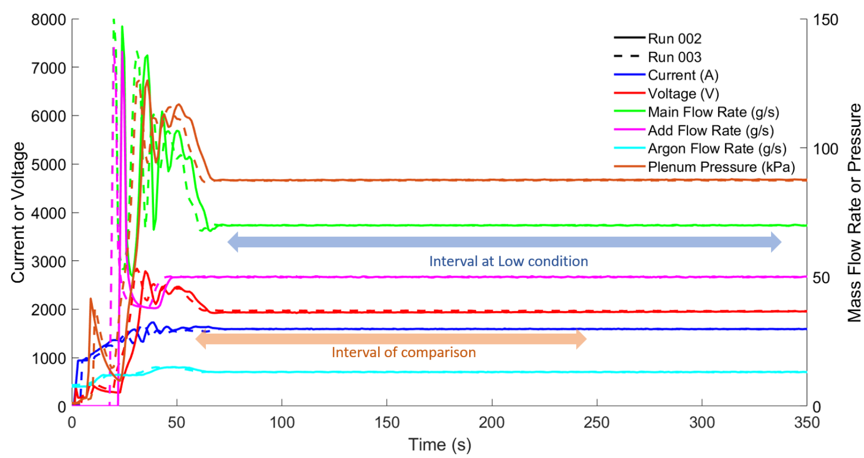

(c)

Fig. 7 Measurements of the temperature at Disk 4 at the Low condition (roughly 1600 A, 2000 V, 0.13 kg/s total flow rate) using O* absorption (left) and N* absorption (right). Measurements are combined from two sequential runs of the IHF. In the first run, N* beams occupied LOS A and D and O* beams occupied LOS B and C. Between runs, this arrangement was inverted. Due to low signal, O* temperature measurements are only attempted on LOS A-C, and N* temperature measurements only on LOS B. Temperature measurements are constrained to around the test times of the respective runs, when the IHF achieved and sustained the Low condition. At bottom, facility-recorded traces of current, voltage, pressure, and flow rate based on nominal input values, with time interval at-condition denoted.

In Fig 7, the measured path-averaged temperatures from O* and N* absorbance from the Low condition on Disk 4 are plotted. Measurements presented in Fig 7 are again an aggregate of two runs, IHF test series 389, runs 002 and 003. In the former run, the beams were arranged with N* beams on LOS A and LOS D and O* beams on LOS B and C, and the beams were then inverted for the second run. The Low condition is at the lower range of achievable conditions in the arcjet, with plenum pressure around 1 atm and flow rate ~15% that of the High condition. Accordingly, absorption signal levels are significantly lower than the other two reported conditions. Centerline measurements of O* and N* were sufficiently robust to estimate a path-averaged temperature of 6000-6200 K. No other lines of sight yielded N* absorbance time histories with adequate SNR to estimate temperature. Temperature inferences were possible on lines of sight A and C using O* absorbance, albeit with high uncertainty; the noise floor for absorption measurements on the A and C paths at a pressure near 1 atm is roughly 5500 K. Temperatures on these lines of sight differ from each other on the order of 100-200 K, though they agree within uncertainty. Measurements in the prior works have sometimes shown evidence of radial non-uniformity, though, with the inclusion of the mixing volume, such variations ought to have been greatly reduced. At this lower IHF condition, it is possible that small run to run discrepancies in the arc dynamics may amplify discrepancies in the data, given the extremely small Boltzmann fraction in the O* ^{5}S state at these relatively low temperatures. Future efforts aim to make measurements at an alternative Low condition (2600 A, 2700 V, 0.24 kg/s), whose larger flow rate should increase signal to noise and improve measurement confidence.

E. Radial Temperature and Measurements of Enthalpy

The O* and N* line of sight temperature inferences above evidence the long-term stability of the IHF at its specified test conditions. Sub-second fluctuations in the absorbance levels, and hence the inference of temperature, have been detected across all IHF conditions. However, these fluctuations are stochastic and relatively steady. IHF runs last on the order of minutes to tens of minutes, over which time the gas flow condition consistently demonstrates stability. This trait lends itself to temporal averaging across the test time intervals in Figs 5,6, and 7. In Fig 8, O* and N* inferred temperature time averages are plotted for the Low, Medium, and High conditions. The x-axis plots the spatial radial location of the A, B, C, and D lines of sight from left to right. The three different conditions span a temperature range from ~5600 K to 7200 K. Temperature homogeneity in these measurements is typically superior to prior works, especially before the mixing volume was included, in that measurements at LOS D (closest to the wall) for one condition are hotter than the LOS B (centerline) for the next hottest condition. Radial temperature gradients do appear to slightly increase in the colder and less dense conditions. Measurements of N* and O* temperature track each other relatively, but are distinct. These differences are sometimes within uncertainty, but always between 100-150 K, corresponding to 1.5-2.5%.

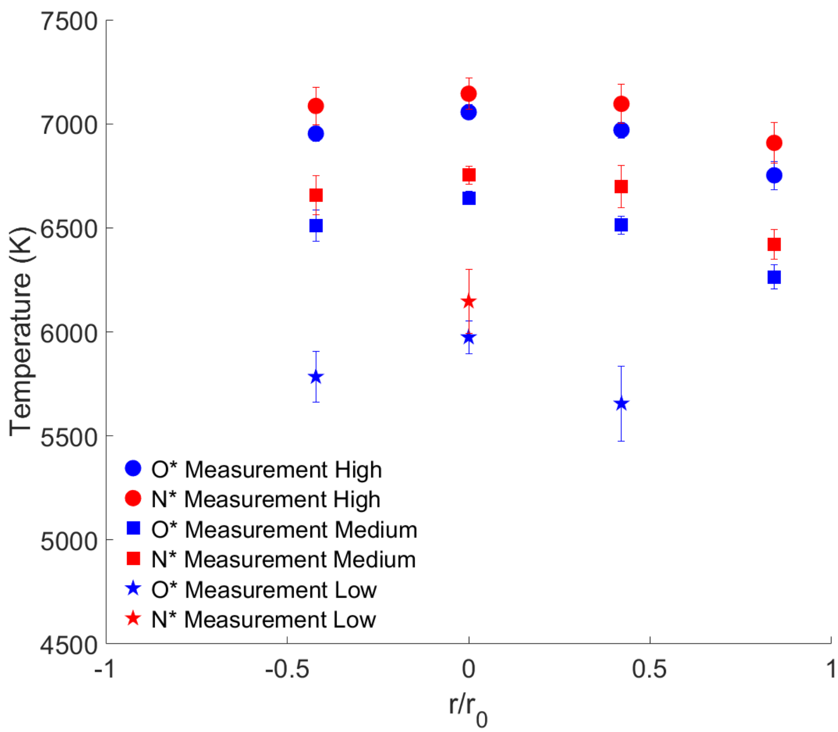

Fig. 8 Time-averaged measurements of temperature from O* and N* absorbance as a function of radial position across the IHF conditions analyzed in this study.

Given the aforementioned assumptions implicit in the single-line temperature methodology, a measurement of temperature implies a measurement of specific enthalpy. This is because, under the constraint of thermal and chemical equilibrium and given a starting chemical composition and a pressure, a measurement of temperature fixes the themodynamic state of the gas. In Fig 9, the radial temperature measurements are converted into specific enthalpy. The measurements in Fig 9 are strictly the internal enthalpy of the flow (chemical and sensible components) and do not include a kinetic component. However, the velocity of the flow at Disk 4 (before nozzle expansion) is on the order of 200-300 m/s and therefore the kinetic energy contribution is negligible. The enthalpy measurements in Fig 9 can thus be interpreted as the stagnation enthalpies of the IHF flows in the considered runs. The time-averaged enthalpy profiles trend similarly to their corresponding radial temperature profiles. However, the discrepancies between conditions, as well as the uncertainty in the measurements, differ due to the non-linear dependence of enthalpy on temperature. At the temperature and pressure ranges in the IHF add-air plenum, molecular oxygen is totally dissociated but molecular nitrogen is not. The extent of uncertainty in the degree of dissociation from the measured absorbance time histories is borne heavily on the enthalpy inference.

The measured enthalpies span a range from 12-19 MJ/kg across conditions. As all of these measurements are on Disk 4, the final optical access point before the nozzle, this enthalpy represents the closest measurement available to the freestream flow in the test chamber. Undoubtedly, enthalpy declines through the mixing volume between the cathode and Disk 4. Future work will present additional measurements taken at upstream disks to evaluate enthalpy loss employing both O* and N* line of sight inferences.

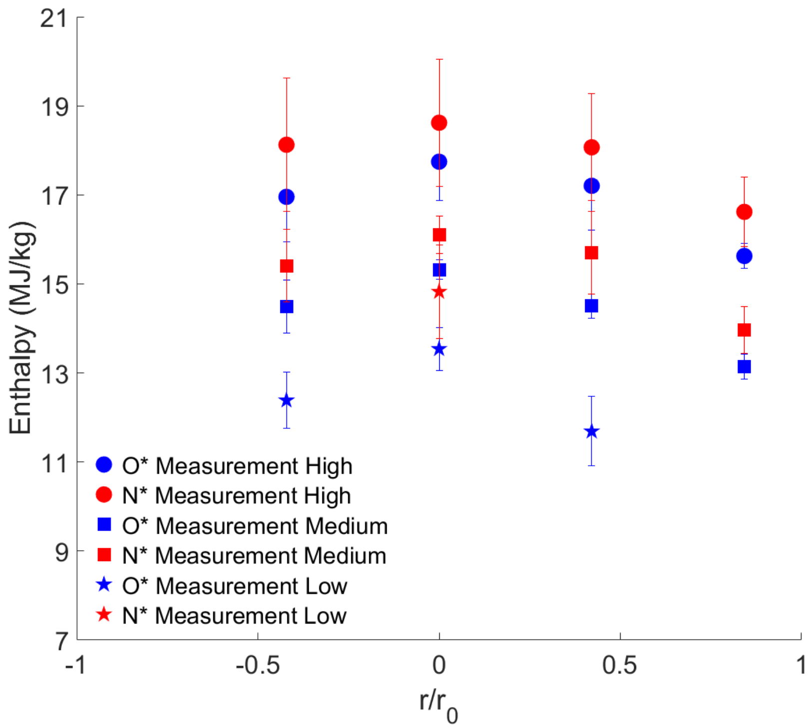

Fig. 9 Time-averaged measurements of specific enthalpy from O* and N* absorbance as a function of radial position across the IHF conditions analyzed in this study.

F. Sensor Performance over a Multi-Condition Run

Thus far, temperature inferences using O* and N* absorbance have been presented at time intervals coinciding with stable IHF operation at a single nominal condition. Certain IHF runs, however, involve variable flow conditions as a function of time. In Fig 10, an IHF run spanning 12 distinct conditions is depicted over a test period of ~ 30 minutes. The conditions begin at an arc setting lower than the Medium condition and terminate at a condition approaching, though still lower than, the High condition. Temperature inferences using the O* beams on the A and B lines of sight are co-plotted along with the facility-provided measurements. Over the course of the run, temperature increases incrementally from 6400 K to close to 7000 K. The time interval of closest approach to the Medium condition is highlighted; this occurs approximately 11 minutes into the run. Temperature inferences at this time interval (~ 6700 K on centerline and ~ 6550 K on the intermediate line of sight) coincide well with the independent measurements taken at the Medium condition as shown in Fig 6. At the end of the run, the centerline temperature of ∼ 7000 K sits 100 K lower than those presented in Fig 5, though the arc current sat about 500 A lower than the High condition.

The relative agreement between inferred temperature measurements across different IHF runs at comparable arc conditions gives good indication as to the repeatability of the IHF facility flow after the mixing volume. This run also underscores that the facility characterization herein is only a limited sample of the wide-range of enthalpies possible in the IHF. The laser system employed in this study demonstrates sufficient sensitivity to the vast majority of these conditions, with at least one spectroscopic transition (N* or O*) measurable in every run that the laser system has been deployed.

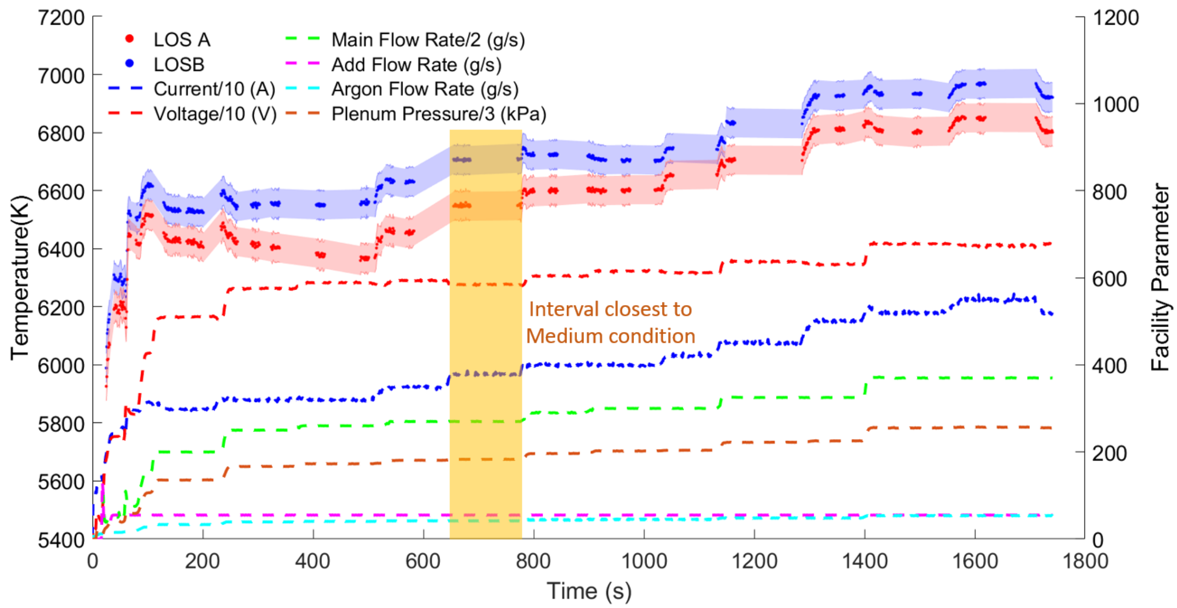

Fig. 10 Measurements taken during IHF Test 382, Run 001, spanning 12 IHF conditions over nearly 30 minutes of test time. LOS A and B O* inferred temperature measurements are co-plotted along with facility-provided measures of current, voltage, mass flow rate, and pressure. The time interval coinciding with the condition closest to the Medium condition is highlighted.

VI. Conclusion

We report on absorption measurements of the reservoir condition in the 60-MW IHF Arcjet at NASA Ames. These measurements are a continuation of a series of spectroscopic characterizations of the IHF facility. Previous surveys have focused on the size of the add-air module as a mixing length to achieve desired spatial uniformity prior to nozzle expansion. In this work, improved laser diagnostics were deployed to more accurately measure temperature and enthalpy in the reservoir to verify this uniformity. Like in previous works, absorption from O*, an electronically-excited state of atomic oxygen, formed the basis of these measurements. New in this work, absorption from N* was used to complement O* absorption, and glean information about the chemical composition of the gas in the reservoir. The absorption from these two species more rigidly constrains the thermodynamic state of the reservoir than either one alone, and permits a measurement of the chemical uniformity, in addition to the spatial uniformity, of the arc flow.

Measurements were taken at 3 nominal conditions, a Low condition (1600 A, 2000 V, 0.13 kg/s), a Medium condition (3500 A, 5700 V, 0.61 kg/s), and a High condition (5900 A, 6800 V, 0.84 kg/s). Data was collected on 'Disk 4', the most downstream disk before the nozzle still offering optical access. Measurements indicate an axi-symmetric flow with a centerline path-averaged temperature of ~7100 K in the High condition, ~6700 K in the Medium condition, and ~6000 K in the Low condition. Radial temperature variation over the lines of sight (from B to D) is found to be ~300 K in the High and Medium conditions. Temperature measurements in the Low condition are challenged by reduced signal quality due to the colder flow and smaller mass flux. Accordingly, only centerline (B) and intermediate (A/C) line of sight O* temperature measurements and centerline line of sight N* temperature measurements are attempted. Independent temperature measurements of O* and N* generally concur across conditions within ~2%, however, N* temperature is persistently higher by 100-200 K.

Temperature measurements were found to be steady at the nominal test conditions. This steadiness permitted temporal averaging across IHF runs and radial 'best-estimate' temperature profiles. Given the assumptions underlying the temperature inferences, specific enthalpy in the reservoir could also be estimated. Centerline enthalpies ranged from 13-18 MJ/kg, with estimates using N* absorption again sitting higher than O* absorption. The discrepancies were often within uncertainty, but nevertheless typify the challenges associated with using excited electronic states to infer thermodynamic properties.

The results in this manuscript focus on measurements of radial uniformity in the IHF in the mixing volume. Additional measurements of O* and N* absorption were taken at several upstream disks closer to the cathode. Future manuscripts will present a more complete picture of the spatial and chemical uniformity of the IHF flow through the add-air plenum by coupling those measurements with the results presented herein.

Acknowledgments

This work was supported under NASA grant number 80NSSC19M0203 with Dr. George Raiche as Technical Officer. This research is only possible with the support of the Thermophysics Facilities Branch, who generously accommodate our project despite its disruption to the normal operation of the IHF. We would like to express our sincere gratitude to the entire IHF staff, in particular test engineers Imelda Terrazas-Salinas, Frank Hui, and Cynthia Sarmiento, facility manager Peter Race, facility operator Antonio Cervantes, and electrician John Anacleto.

References

[1] Nations, M., Chang, L. S., Jeffries, J. B., Hanson, R. K., MacDonald, M. E., Nawaz, A., Taunk, J. S., Gökçen, T., and Raiche, G., "Characterization of a large-scale arcjet facility using tunable diode laser absorption spectroscopy," *AIAA Journal*, Vol. 55, No. 11, 2017, pp. 3757–3766.

[2] Viveros Salazar, D., Strand, C. L., Hanson, R. K., and MacDonald, M. E., "Investigating Arcjet Mixing and Enthalpy Loss Using Atomic Oxygen Laser Absorption Spectroscopy," *AIAA Journal*, Vol. 60, No. 2, 2022, pp. 976–984.

[3] Stewart, D., Gokcen, T., and Chen, Y.-K., "Characterization of Hypersonic Flows in the AHF and IHF of NASA Ames Arc-Jet Facilities," *41st AIAA Thermophysics Conference*, 2009, p. 4237.

[4] Winter, M., Raiche, G., Terrazas-Salinas, I., Hui, F., White, B., and Taunk, J., "Measurements of Radiation Heat Flux to a Probe Surface in the NASA Ames IHF Arc Jet Facility," *43rd AIAA Thermophysics Conference*, 2012, p. 3189.

[5] Grinstead, J., Raiche, G., and Gökçen, T., "Test Engineering for Arc Jet Testing of Thermal Protection Systems: Design, Analysis, and Validation Methodologies," *25th AIAA Aerodynamic Measurement Technology and Ground Testing Conference*, 2006, p. 3290.

[6] Balter-Peterson, A., Nichols, F., Mifsud, B., and Love, W., "Arc jet testing in NASA Ames Research Center thermophysics facilities," *AIAA 4th International Aerospace Planes Conference*, 1992, p. 5041.

[7] Myers, D. E., *Parametric weight comparison of advanced metallic, ceramic tile, and ceramic blanket thermal protection systems*, National Aeronautics and Space Administration, Langley Research Center, 2000.

[8] Grinstead, J., Wilder, M., Olejniczak, J., Bogdanoff, D., Allen, G., Dang, K., and Forrest, M., "Shock-heated air radiation measurements at lunar return conditions," *46th AIAA aerospace sciences meeting and exhibit*, 2008, p. 1244.

[9] Berger, K. T., Hollingsworth, K. E., Wright, S. A., and Rufer, S. J., "NASA Langley Aerothermodynamics Laboratory: hypersonic testing capabilities," *53rd AIAA aerospace sciences meeting*, 2015, p. 1337.

[10] ROCHELLE, W., BATTLEY, H., GRIMAUD, J., TILLIAN, D., MURRAY, L., LUEKE, W., and HEATON, T., "Orbiter TPS development and certification testing at the NASA/JSC 10MW Atmospheric Reentry Materials and Structures Evaluation Facility," *21st Aerospace Sciences Meeting*, 1983, p. 147.

[11] Smith, D., Felderman, E., Shope, F., and Balboni, J., "Arc-Heated Facilities," *Progress in Astronautics and Aeronautics*, Vol. 198, 2002, pp. 279–314.

[12] Lu, F. K., and Marren, D. E., "Principles of hypersonic test facility development," *Progress in Astronautics and Aeronautics*, Vol. 198, 2002, pp. 17–28.

[13] Smith, R., Wagner, D., and Cunningham, J., “A survey of current and future plasma arc-heated test facilities for aerospace and commercial applications,” *36th AIAA Aerospace Sciences Meeting and Exhibit*, 1998, p. 146.

[14] Terrazas-Salinas, I., and Cornelison, C., “Test Planning Guide for NASA Ames Research Center Arc Jet Complex and Range Complex,” *Space Technology Division, NASA Ames Research Center, Moffett Field, CA*, Vol. 94035, 2009, pp. 20–21.

[15] Prabhu, D., Saunders, D., Oishi, T., Skokova, K., Santos, J., Fu, J., Terrazas-Salinas, I., Carballo, J., and Driver, D., “CFD analysis framework for arc-heated flowfields I: stagnation testing in arc-jets at NASA ARC,” *41st AIAA Thermophysics Conference*, 2009, p. 4080.

[16] Park, C., Raiche, G. A., Driver, D. M., Olejniczak, J., Terrazas-Salinas, I., Hightower, T. M., and Sakai, T., “Comparison of enthalpy determination methods for an arc-jet facility,” *Journal of thermophysics and heat transfer*, Vol. 20, No. 4, 2006, pp. 672–679.

[17] Palmer, G., Prabhu, D. K., and Terrazas-Salinas, I., “Arc Jet Facility Test Condition Predictions Using the ADSI Code,” *45th AIAA Thermophysics Conference*, 2015, p. 2663.

[18] Hanson, R. K., Spearrin, R. M., and Goldenstein, C. S., *Spectroscopy and Optical Diagnostics for Gases.*, Springer International Publishing, 2016.

[19] Kramida, A., Yu. Ralchenko, Reader, J., and and NIST ASD Team, NIST Atomic Spectra Database (ver. 5.9), [Online]. Available: `https://physics.nist.gov/asd` [2022, May 23]. National Institute of Standards and Technology, Gaithersburg, MD., 2021.

[20] Irwin, A. W., “Polynomial partition function approximations of 344 atomic and molecular species,” *The Astrophysical Journal Supplement Series*, Vol. 45, 1981, pp. 621–633.

[21] Li, Y., Wang, S., Strand, C. L., and Hanson, R. K., “Two-temperature Collisional-radiative Modeling of Partially Ionized O2–Ar Mixtures over 8000–10,000 K Behind Reflected Shock Waves,” *The Journal of Physical Chemistry A*, Vol. 124, No. 19, 2020, pp. 3687–3697.

[22] Finch, P. M., Granowitz, Z. N., Streicher, J. W., Krish, A., Strand, C. L., and Hanson, R. K., “Shock-Tube Measurements of Atomic Nitrogen Collisional Excitation in 8000-12000 K Partially-Ionized Nitrogen-Argon Mixtures,” *The Journal of Physical Chemistry A*, 2022, submitted.

[23] McBride, B. J., *NASA Glenn coefficients for calculating thermodynamic properties of individual species*, National Aeronautics and Space Administration, John H. Glenn Research Center, 2002.

[24] Winter, M., Prabhu, D., Taunk, J., and Terrazas-Salinas, I., “Emission spectroscopic measurements in the plenum region of the NASA IHF arc jet facility,” *10th AIAA/ASME Joint Thermophysics and Heat Transfer Conference*, 2010, p. 4522.

[25] Winter, M., Prabhu, D. K., and Williams, W. W., “Radiation transport analysis of emission spectroscopic measurements in the plenum region of the NASA IHF arc jet facility,” *45th AIAA Plasmadynamics and Lasers Conference*, 2014, p. 2489.